Electron density and ionization dynamics in an imploding *z*-pinch plasma

L. Gregorian, E. Kroupp, G. Davara,[a] V. I. Fisher, A. Starobinets, V. A. Bernshtam,
A. Fisher,[b] and Y. Maron
Faculty of Physics, Weizmann Institute of Science, Rehovot, 76100, Israel

The time-dependent radial distributions of the electron and ion densities during the implosion phase of a gas-puff *z*-pinch plasma are determined from measurements of continuum radiation, as well as time-dependent collisional-radiative analysis of the observed particle ionization history in the plasma. It is shown that during the 140-ns-long time interval close to the end of the ~620-ns-long implosion phase, the total imploding-plasma mass increases by ~65%, found to be consistent with the continuous ionization of the gas ahead of the plasma shell. Furthermore, the densities obtained, together with the previously determined radial distributions of the electron temperature, magnetic field, and particle radial velocities, are used to analyze the energy terms that support the radial propagation of the ionization wave seen in the plasma, thereby explaining the time-dependent radial distribution of the ion charge states in the plasma. © *2005 American Institute of Physics.*
[DOI: 10.1063/1.2039943]

I. INTRODUCTION

In imploding *z*-pinch plasmas,[1–5] knowledge of the particle density history is of key importance for studying the interaction between the plasma and the magnetic field. In particular, the plasma properties and the x-ray radiation characteristics at stagnation are considerably affected by the implosion dynamics. Therefore, understanding the processes that govern the plasma implosion requires a reliable determination of the particle density as a function of time and radius.

The methods most commonly employed for the determination of the electron density n_e in plasmas are measurements of continuum radiation and Stark broadening of spectral lines.[6,7] However, the former technique lacks, in most cases, the spatial resolution required for obtaining the radial distribution of n_e, while the latter, when applied to the study of imploding plasmas such as the *z*-pinch, may be prone to difficulties in the data interpretation due to the effects of opacities and ion velocities on the line shapes.[8]

In this article, we present a method for determining the radial distributions of the electron and ion densities in the plasma during the implosion using analysis of the ionization times of atoms and ions in the plasma, obtained from end-on, spatially resolved observations of line intensities of oxygen ions up to O VI. The analysis is based on collisional-radiative (C-R) calculations,[9] and on the observed radial distributions of the ion radial velocities[5] and the electron temperature T_e.[10] The particle densities are then obtained from the comparison of the calculated radial distribution of the ion mean ionization degree $Z(r,t)$ to the observed one. The electron density n_e within the dense and hot region at the outer boundary of the plasma shell is also determined independently using measurements of the absolute continuum intensity. The density obtained, together with the observed $T_e(r,t)$ and the magnetic-field radial distribution,[11] are then used to estimate the energy balance in the gas-plasma interface and in different radial regions of the plasma, which helps to explain the radial propagation of the ionization wave, previously observed for this plasma.[5]

In the following, the experiment is described in Sec. II, the continuum measurements in Sec. III, and the analysis of the particle ionization in Sec. IV. The discussion on the radial propagation of the ionizations in the plasma is given in Sec. V.

II. EXPERIMENT AND DIAGNOSTICS

The *z*-pinch system and the diagnostics setup used here are described elsewhere.[5,10] In brief, a 30-kV, 320-kA, 1-μs capacitor-bank discharge circuit powers the implosion of an annular, cylindrical plasma produced by a gas-puff device. For the CO_2 plasma under study, the time of maximal compression is $t\sim620$ ns ($t=0$ is the beginning of the discharge), and the plasma radial motion takes place mostly between $t\sim400$ and 570 ns. During this period, the plasma ionizes continuously up to O VI, forming a radial distribution of the charge Z for which at each instant the singly charged ions reside at the smallest radii, and the radial positions of the higher charge states are larger for a higher Z.[5]

The spatial distribution of the gas mass density prior to the application of the current pulse was obtained from measurements using miniature, calibrated ionization (Penning) probes, which were positioned in front of the nozzle (cathode) at various radial and axial locations. The cross-sectional area of the probes perpendicular to the gas axial flow was $\simeq3$ mm, which thus defined the spatial (radial) resolution. Given in Fig. 1 are examples of the gas-density distribution obtained for three axial locations within the anode-cathode gap. Such measurements yielded that the linear mass density of the gas was 10 ± 3 μg/cm. In addition, simultaneous probe measurements at several azimuthal locations for the same axial and radial positions were used to examine the gas shell uniformity, giving gas-density variations below 5%.

---

[a] Also at Orbotech Ltd., Yavne, Israel.
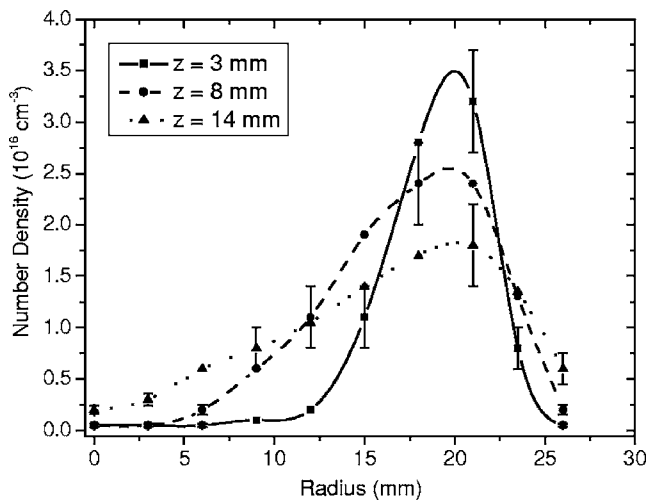[b] Also at Technion-Israeli Institute of Technology, Haifa, Israel.

FIG. 1. The initial gas-density distribution prior to the plasma implosion, measured at three axial locations (the nozzle is at $z=0$). The nozzle radius is 20.0 mm.

The diagnostics employed is a UV-visible (2000–7000 Å) spectroscopic system, consisting of a 1.3-m spectrometer and a high-speed streak camera, lens-coupled to a charge-coupled device (CCD). For the present study, the input optics were configured for end-on observations of the plasma, i.e., with the line of sight parallel to the z axis at various radial positions. In such a configuration, the spatial resolution along the radial (horizontal) dimension of the plasma varied from $\Delta r=0.5$ to 1.9 mm, depending on the input slit width. The resolution along the azimuthal dimension of the plasma, which for the radial positions used here is nearly parallel to the vertical dimension of the spectrometer input slit, was $\Delta h=2.5$ mm. As a result of the plasma axial nonuniformity (see Refs. 10 and 11), the integration length L along the line of sight varied, depending on the spatial (radial) resolution chosen. A schematic of the configurations of the end-on observation, employing the two options for the spatial resolution in the radial direction, is given in Fig. 2. Shown in the figure is the shape in the r-z plane of the plasma shell at a given time (solid lines) and the field of view of the spectroscopic system (dotted lines). It is seen that the length L of the plasma region observed (the gray area) depends on the resolution used. More specifically, L was found to be $\sim$4.0 mm (extending from the anode) in the high-resolution measurements ($\Delta r=0.5$ mm) and 9.0±4.0 mm in the low-resolution measurements ($\Delta r=1.9$ mm). The temporal resolution was 10 ns throughout the experiments. The spectral resolution varied between 0.1 Å for the line-intensity measurements to $\sim$1.0 Å for the continuum measurements.

III. CONTINUUM-RADIATION MEASUREMENTS

The emission of continuum radiation is observed throughout the plasma implosion. During the time interval studied here, the range of n_e in the plasma shell, expected from the measured initial gas-density distribution, is 2.0×10^{16}–1.0×10^{18} cm^{-3}.[12] The range of T_e, as determined using measurements of line-intensity ratios described in Ref.
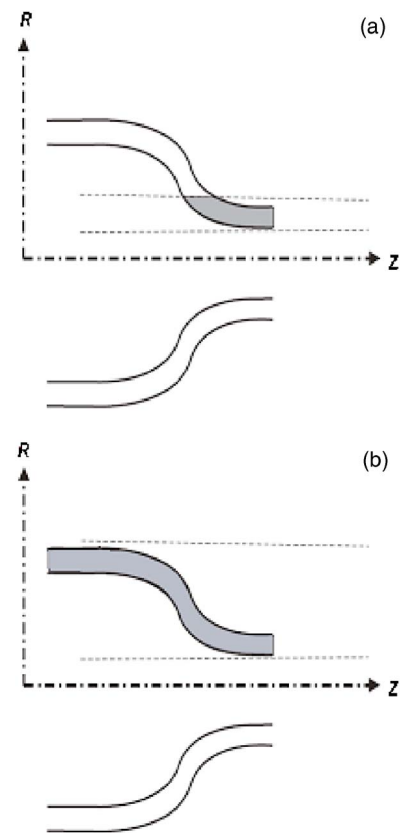

FIG. 2. The spatial shape of the plasma in the r-z plane at a given time (solid lines) together with the field of view of the spectroscopic system (dotted lines) in (a) the high-spatial-resolution and (b) the low-resolution observations.

10, is 5–14 eV. For these parameters, the continuum emission in the spectral region of 3000–5000 Å is dominated by bremsstrahlung (free-free) radiation, for which the emission power density is given by[7,13]

$$P_{ff} = 1.9 \times 10^{-28} G_{ff} \frac{Z^2 n_i n_e}{\lambda^2 T_e^{1/2}} e^{hc/\lambda k T_e} \ \text{W cm}^{-3} \ \text{Å}^{-1}. \quad (1)$$

Here, T_e is given in eV, n_i is the ion number density (cm^{-3}), Z is the mean ion charge, λ is the wavelength (in Å), and G_{ff} is the Gaunt factor for free–free transitions,[14] which for the relevant ranges of T_e and λ is between 1.3 and 2.0.

Time-dependent, end-on observations of the continuum radiation were carried out for several instances during the implosion at various radial positions, using several line-free spectral regions between 3000 and 4500 Å. In the measurements, the low radiation intensity required the use of a spatial (radial) resolution Δr between 1.4 and 1.9 mm. Figure 3 gives an example of a measurement of the continuum-intensity history, observed at $r=16.7$ mm and averaged over six identical discharges. It is seen that the intensity peaks at $t=482\pm5$ ns, which is consistent with the fact that at $t=480$ the highest charge states abundant in the plasma (O IV and O V) are both located at $r\simeq17.0$ mm. In more detail, the radial width of the emitting plasma volume can be obtained from the temporal width Δt of the continuum signal multiplied by the known plasma radial flow velocity. For $\Delta t \simeq 65$ ns as in Fig. 3, a typical velocity of 7×10^6 cm/μs, and
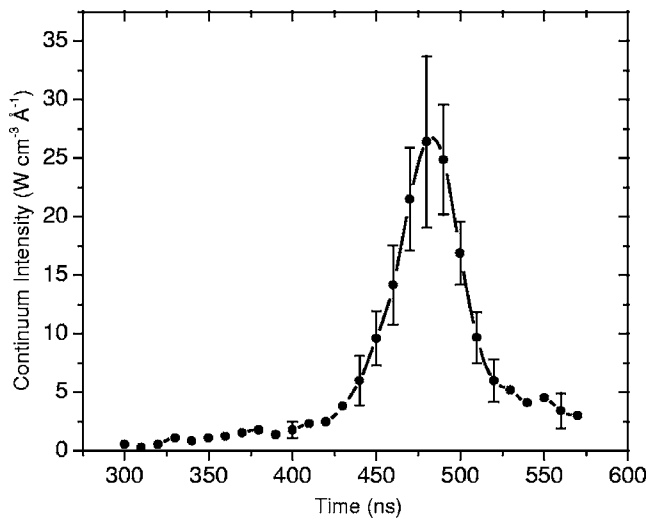
FIG. 3. The absolute continuum intensity measured at $r=10.2$ mm.

accounting for the instrumental resoluion (1.9 mm), this gives a width of ~4 mm, which agrees well with the observed total radial width of the plasma region dominated by O IV and O V.

Table I gives the continuum intensities measured for three times during the implosion, together with the corresponding values of n_e, obtained using Eq. (1) for the known values of $Z(r,t)$.[5] For each time, the data is the averaged intensity obtained from six to ten identical discharges. Based on these results and the known radial width of the highest-charge-state region in the plasma, the linear density of the plasma (mass per unit length), which throughout the paper is referred to as "the plasma mass," is then calculated. The mass obtained gives a lower limit for the mass of the entire plasma shell, since for each instant it is assumed that the main contribution to the continuum emission observed is from the highest-charge-state plasma region. The uncertainties quoted account for both the statistical shot-to-shot variations and the geometrical uncertainties in the plasma due to the integration along z and the plasma shell thickness. Note that for the parameters of the plasma studied here the effect of the continuum self-absorption in the plasma along the line of sight is negligible.

IV. ANALYSIS OF THE IONIZATION IN THE PLASMA

In this section we describe a method for the determination of the electron density by analyzing the ionization of atoms and ions in the plasma. The method is based on the comparison between the time-dependent distribution of the

ion charge $Z(r,t)$ obtained experimentally[5] to the charge-state composition obtained from a C-R modeling.[9] For the calculations, the electron temperature is independently determined from spectral line ratios,[10] and the ion density (or the plasma mass density) is used as a variable parameter. In addition, since the time-dependent charge-state composition as observed along the z axis also depends on the plasma radial flow, the radial distribution of the ion radial velocities $v_r(t)$ (Ref. 5) is accounted for in the model. We note that while the analysis is carried out for oxygen, it was confirmed by C-R calculations that for the present plasma conditions, the carbon ions (that are $<1/3$ of the plasma mass) are of a very similar charge-state distribution as oxygen, justifying that this simplification hardly affects the analysis results.

Several additional assumptions are used for the model. First, the plasma is assumed to be axially and azimuthally uniform, as discussed in Ref. 10. The radial dependence of the plasma-shell parameters is simulated by dividing the plasma into three concentric annular layers with their instantaneous radial positions corresponding to those of the three dominating charge states in the plasma shell. An example of the layer structure for $t=490$ ns is shown in Fig. 4(a). Each layer α is characterized by mean values for the ion charge Z_α, the mass density ρ_α, the electron temperature T_e^α, and the inner and outer radii, $r_{\alpha i}$ and $r_{\alpha o}$, respectively. The model allows for simulating both the rise in time of the total plasma mass and the flow of mass across the boundaries of the layers. The total mass can rise due to the continuous sweeping and ionization of the gas found ahead of the imploding plasma shell (see Sec. III). It is also assumed here that there is no mass "leakage" across the plasma outer boundary, so that the entire ionized gas is imploded. This assumption is based on the fact that the total observed light intensity drops sharply (by orders of magnitude) at a radius $\simeq0.5$ mm larger than that of the highest charge state.

For the analysis, we use the radial distributions of T_e, Z, and v_r, all measured at $t=490$ and 540 ns, except for the value of T_e for layer 2 at $t=490$ ns, which is interpolated. The starting point t_0 for the calculations corresponds to the experimental time $t=400$, for which only part of the data is available, i.e., v_r and Z for the central and outer layers of the plasma. The rest of the parameters, namely v_r and Z for the inner layer and T_e for all three layers, are obtained by extrapolations of the measured data. It will be shown *a posteriori* that these assumptions for the parameters at $t=400$ ns hardly affect the results.

The experimental data used in the calculations for the three layers is given in Table II. These include r_i, r_o, T_e, Z, and v_r, where the latter is specified for the center of each

TABLE I. Experimental data for the continuum intensity and n_e obtained for three times during the implosion. λ is the average wavelength of observation, with the spectral interval $\Delta\lambda$ being ~7 Å in all the measurements.

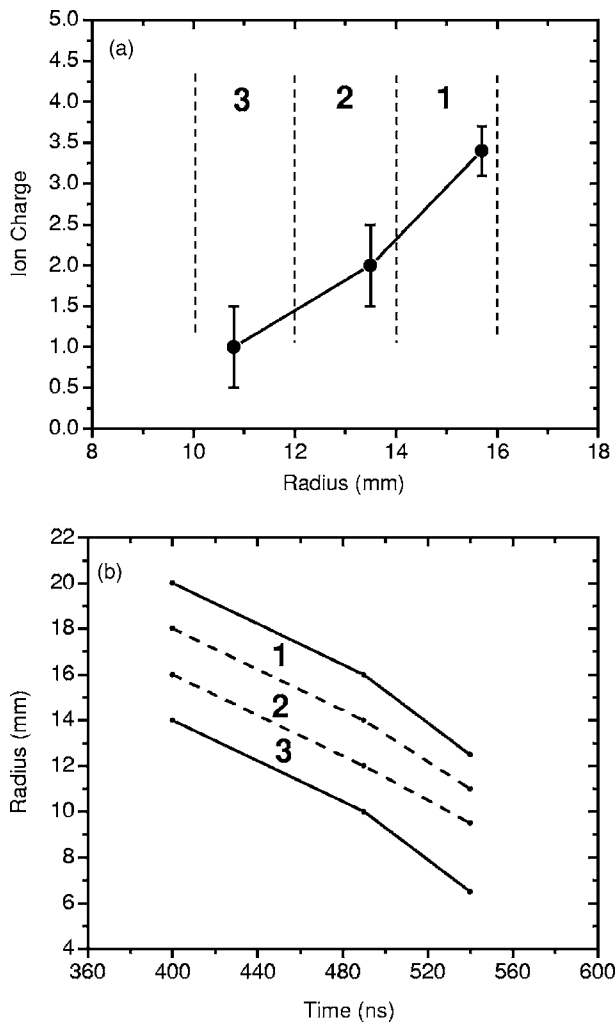| t (ns)	r (mm)	λ(Å)	P_{ff} (W cm^{-3} Å^{-1})	T_e (eV)	$\bar{Z}$	n_e (10^{18} cm^{-3})
480	16.7	3110	26.4±7.3	10.5±0.5	3.5	0.96±0.24
545	10.2	3230	60.4±11.1	13±1	4.5	1.33±0.31
585	6.0	3230	511±80	15±2	5.0	3.5±0.76

FIG. 4. (a) The measured radial distribution of the charge state in the plasma at $t=490$ ns, together with the radial positions of the layers used in the analysis (see text). (b) The time-dependent radial positions of the boundaries of the three layers.

TABLE II. Data used for the calculations.

Time (ns)	Parameters	Outer layer (1)	Central layer (2)	Inner layer (3)
400	r_o (mm)	20.0	18.0	16.0
	r_i (mm)	18.0	16.0	14.0
	T_e (eV)	5.5±0.5	4.3±0.3	3.0±0.2
	$\bar{Z}$	2.0±0.5	1.0±0.1	0.75±0.25
	v_r (10^6 cm/s)	4.0±0.6	2.5±0.4	1.0±0.5
490	r_o (mm)	16.0	14.0	12.0
	r_i (mm)	14.0	12.0	10.0
	T_e (eV)	10.5±0.5	6.5±0.5	4.0±0.2
	$\bar{Z}$	3.3±0.3	1.8±0.3	1.0±0.2
	v_r (10^6 cm/s)	5.5±0.5	3.8±0.4	1.0±0.5
540	r_o (mm)	12.5	11.0	9.5
	r_i (mm)	11.0	9.5	6.5
	T_e (eV)	13.0±1.0	8.5±0.5	5.0±0.2
	$\bar{Z}$	4.5±0.3	2.8±0.4	1.5±0.3
	v_r (10^6 cm/s)	8.0±0.5	5.0±0.4	2.0±0.6

data. For the other two layers, calculations using constant masses give reasonable data fits that are within the experimental uncertainties.

As the next step, mass transport is introduced in order to improve the accuracy of $Z_\alpha^{\text{calc}}(t)$. The time-varying masses for the three layers used in these calculations are determined based on the velocities v_r as follows. We consider a narrow annular layer of thickness δr, which for a given instance t is located at some radial position r between r_α and r_β (the instantaneous positions of the centers of the neighboring layers α and β, respectively). Let us denote the mass of this layer by $\delta m_{\alpha\beta}$. Assuming a linear interpolation, the radial velocity of this layer is

$$v(r,t) = v_\alpha(t) + \frac{v_\beta(t) - v_\alpha(t)}{r_\beta(t) - r_\alpha(t)}[r - r_\alpha(t)], \tag{2}$$

where v_α and v_β are the respective radial velocities of the particles at the centers of the α and β layers (Table II). The radial displacement of the narrow layer at any given instant $t' > t$ is given by

$$r' = r - \frac{v + v'}{2}(t' - t), \tag{3}$$

where $v' = v(r,t')$ is the hydrodynamic velocity of the layer at the time t' obtained from Eq. (2). Using Eqs. (2) and (3), the mass histories for the three layers of the plasma can now be calculated.

As an example for such a calculation, let δm_{12} be initially (at $t=400$ ns) located at the boundary between layers 1 (outer) and 2 (central). Its velocity, according to Eq. (2), is $v_{12}(400)=3.25\times10^6$ cm/s. At $t=490$ ns, δm_{12} will be displaced to some coordinate r'_{12}, for which according to Eq. (2) the velocity is

layer, i.e., for $r=(r_i+r_o)/2$. The radial-position history of the layers is illustrated in Fig. 4(b). Let us denote the masses of the outer, central, and inner layers by $m_1(t)$, $m_2(t)$, and $m_3(t)$, respectively, and the total plasma mass by $M(t)$ (this does not account for the nonionized gas mass). For each layer α, the mass density (per unit volume), related to the mass via $m_\alpha(t) = \pi\rho_\alpha(t)(r_{\alpha o}^2 - r_{\alpha i}^2)$, is used as a variable input parameter in the C-R analysis. The iterative procedure consists of varying $\rho_\alpha(t)$ so that the calculated charge $Z_\alpha^{\text{calc}}(t)$ best fits the experimental values of Z.

As the first step in the analysis, the charge-state history for the time interval of $400 < t < 540$ ns is calculated separately for each layer α using constant values of the masses m_α. The radial velocities v_r are not accounted for in these calculations, so that the mass transport across the layer boundaries is neglected. Examples for the results of such calculations of $Z_\alpha^{\text{calc}}(t)$ using several values of m_α for the three layers are given by the solid curves in Fig. 5, together with the experimental data points at $t=490$ and 540 ns. It is seen that for the outer layer [Fig. 5(a)], a calculation using a constant mass of ~ 4.0 μg/cm provides a very good fit to the
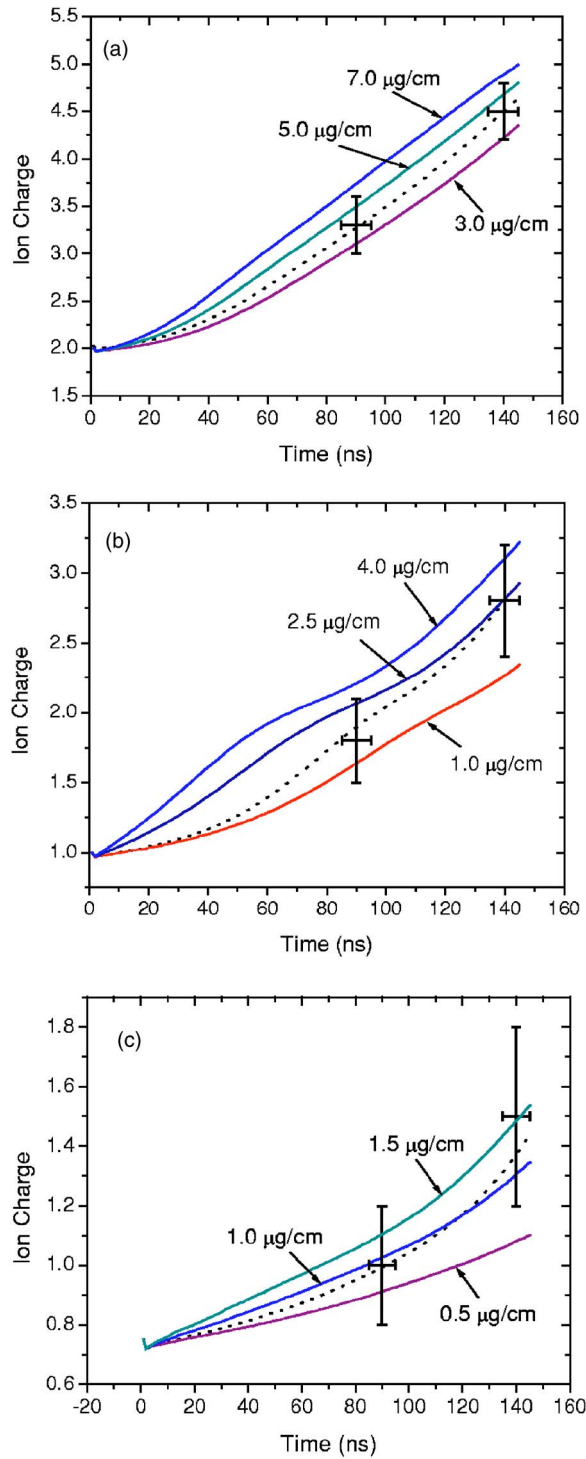
FIG. 5. The time histories of the charge for the (a) outer, (b) central, and (c) inner layers of the plasma, each calculated for several constant values of the mass line density ρ. Also given are the experimental values of the mean charge state for each layer, measured at $t=490$ and 540 ns, together with the best-fit calculations using a time-dependent mass which accounts for the mass flow into and out of the plasma layer (see text).

TABLE III. Best-fit linear mass densities assumed and the calculated electron and ion number densities for the three layers.

Time (ns)	Parameters	Layer 1	Layer 2	Layer 3
400	Mass (μg/cm)	3.5 ± 0.7	1.0 ± 0.3	0.65 ± 0.2
490	Mass (μg/cm)	3.6 ± 0.6	2.0 ± 0.5	1.05 ± 0.15
	n_i (10^{17} cm^{-3})	0.72 ± 0.12	0.47 ± 0.11	0.28 ± 0.05
	n_e (10^{17} cm^{-3})	2.4 ± 0.48	0.85 ± 0.22	0.28 ± 0.05
540	Mass (μg/cm)	4.0 ± 0.6	2.9 ± 0.6	1.6 ± 0.5
	n_i (10^{17} cm^{-3})	1.35 ± 0.2	1.11 ± 0.22	0.4 ± 0.1
	n_e (10^{17} cm^{-3})	6.1 ± 1.0	3.1 ± 0.7	0.6 ± 0.2

ary between layers 1 and 2 is positioned at $r=14.0$ mm. The extra shift of 0.3 mm in r_i of the outer layer can be explained therefore by partial addition of particles from the central layer due to ionization. Since for both cases, i.e., $m_1(400)$ at $t=490$ and $m_1(490)$, ρ_1 is identical, the resulting gain in the mass of m_1 over the 90 ns interval is calculated using the ratio of the layer boundaries. For the present example this ratio is $(1.6^2-1.4^2)/(1.6^2-1.43^2)$, and the resulting mass gain is given by $m_1(490)\simeq1.17m_1(400)$.

Repeating the calculation for δm_{12} between $t=490$ and 540 ns then allows the total gain in the mass of the outer boundary to be obtained, which is given by the relation $m_1(540)\simeq1.28m_1(400)$. Following the same procedure, we calculate the radial displacement of different mass units in order to determine the total gain in m_2 and m_3 during the 400–540 ns time interval, and these results are given by the relations $m_2(540)=2.77m_2(400)$ and $m_3(540)=2.46m_3(400)$.

Having determined the time evolution of $m_\alpha(t)$ for each layer, iterative C-R calculations are carried out for each layer separately by varying the initial values of the masses, i.e., $m_\alpha(400)$, and comparing the calculated charge $Z^{\text{calc}}(t)$ with the experimental values at $t=490$ and 540 ns. The results of the best-fit calculations using the time-dependent masses for the three layers are given by the dashed curves in Fig. 5.

The results of the mass calculations for variable initial conditions are summarized in Table III. The radial distributions of n_e and n_i given in the table are illustrated in Fig. 6. It is seen from these results that the total mass of the imploding plasma increases by $\sim$65% during the 140-ns-long interval studied here.

V. DISCUSSION

It was shown in Ref. 5 that for the plasma under study an ionization wave propagates radially inward faster than the plasma hydrodynamic radial flow. The radial distributions of the electron and ion densities determined in the above, together with the known radial distributions of T_e (Ref. 10) and the magnetic field,[11] allow now for examining the energy terms required to support the propagation of the ionization, which helps explaining the charge-state distribution observed across the plasma shell.[5]

$$v'_{12}(490) = v_2(490) + \frac{v_1(490)-v_2(490)}{r_1(490)-r_2(490)}[r'_{12}-r_2(490)].$$

$$(4)$$

Substituting $v_{12}(400)$ and $v'_{12}(490)$ into Eq. (3) gives $r'_{12}(490)=14.3$ mm. For comparison, at $t=490$ ns the bound-
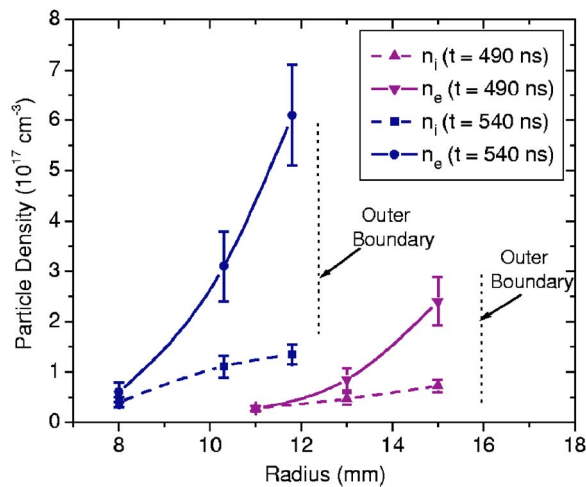
FIG. 6. The radial distributions of the electron and ion densities in the plasma for two times during the implosion.

First, we show that the ionization of atoms (O I) occurs due to the continuum-radiation emission from the hot, outer region of the plasma. The photoionization rate of an atom in a quantum state α is given by

$$W_{p-i}^{\alpha} = \int_{(4\pi)} \int_{E_\alpha}^{\infty} \sigma_{p-i}^{\alpha}(\nu) \frac{I_\nu(\mathbf{\Omega})}{h\nu} d\nu d\mathbf{\Omega}, \tag{5}$$

where E_α is the ionization potential, ν is the radiation frequency, $I_\nu(\mathbf{\Omega})$ is the specific plasma radiation intensity in the direction $\mathbf{\Omega}$, and $\sigma_{p-i}^{\alpha}(\nu)$ is the photoionization cross section.[15] $I_\nu(\mathbf{\Omega})$ is the solution of the radiative-transfer equation, and it is obtained self-consistently from the C-R calculations. The photoionization probability is obtained by summation of the rates [Eq. (5)] over the quantum states, i.e., $W_{p-i} = \Sigma_\alpha f_\alpha W_{p-i}^{\alpha}$, where f_α is the fraction of the atoms in quantum state α and $\Sigma_\alpha f_\alpha = 1$.

The photoionization calculations can be compared to the experimentally obtained time scale of the radial propagation of the ionization, therefore it is more convenient to use the mean photoionization times defined as $\tau_{p-i} = 1/W_{p-i}$. The observed velocity v_f of the ionization-wave front (O I–O II interface) during the time period between $t \simeq 400$ and 570 ns is $\sim 9 \times 10^6$ cm/s,[5] which means that the ionization time scale is $\simeq 10$ ns for a given 1-mm-thick plasma (gas) region. For comparison, calculations using the known values of n_e (see Sec. IV) and T_e (given in Ref. 10) in the plasma for $t \simeq 440$, 490, and 540 ns, yield $\tau_{p-i} \sim 7$, ~ 2, and ~ 1 ns, respectively. Therefore, since these times are faster than the experimental time scale, one may conclude that the radiation from the hot plasma region can support the continuous ionization of atoms at the inner boundary of the plasma during the implosion.

We note here that since the mean free path for the photoionizing radiation is longer than the radial width (thickness) of the gas shell, the ionization of O I is expected to occur over the entire gas. However, in our experiment line emission from O II peaks at different times for different radial locations, i.e., the O II radiation is seen as a radially propagating front. This can be explained by the fact the O II

UV lines used for the measurements correspond to atomic transitions between relatively high energy levels of O II, which are populated due to electron-impact excitations at the inner region of the plasma shell. Thus, the O II-radiation propagation results from the propagation of the electron heating.

A detailed investigation of the energy-deposition history in the plasma during the implosion is given in Ref. 10. Here we use the deposition rates obtained, and the data presented above, for studying the ionization dynamics within the plasma shell. During the 440–570 ns interval, the radial separation of the charge states remains unchanged and the ionization front velocity v_f is nearly constant, which therefore allows for a steady-state energy balance analysis to be employed. In addition, a planar geometry is assumed, since for the times and the radial region presently considered the cylindrical terms are estimated to bear a little effect.

As an example, let us examine the propagation of the O II ionization (into O III) in the plasma. For this examination, we start with the equation for the internal energy ε in the one-dimensional (1D) magnetohydrodynamic approximation (see, e.g., Ref. 16). First, it is assumed that since the radial hydrodynamic velocity of O II ions, $<1 \times 10^6$ cm/s, is small compared to v_f,[5] it can be neglected. It is then more convenient to carry out the calculation in the reference frame of the moving planar ionization front, comparing energy fluxes within a plasma slab of a thickness Δr. Based on these assumptions, the energy equation may be converted to

$$v_f \frac{\Delta \varepsilon}{\Delta r} = \frac{v_f}{\Delta r}\left(n_i^{+1} I_{\text{ion}} + \frac{3}{2}(n_e T_e + n_i^{+1} T_i)\right) = \eta J_z^2 - p\frac{\Delta u}{\Delta r}, \tag{6}$$

where n_i^{+1} is the ion density of O II, v_f is the ionization front velocity, η is the electrical resistivity, J_z is the axial current density, $p = p_e + p_i$ is the thermal pressure, and I_{ion} is the ionization energy per an O II particle, which is ~ 35 eV (it is assumed that all O II particles are in their ground state). The right-hand-side (rhs) terms of Eq. (6) are the Joule heating and the compressional heating, respectively, and these are determined in Ref. 10. It should be mentioned here that the energy deposition due to the electron heat flux, calculated based on the electron-temperature gradient in the plasma, is found to be negligibly small.[10] Evaluation of v_f is carried out using the data given in the above and in Ref. 10. Calculation for $t \simeq 540$ ns using $\Delta r = 3$ mm, $n_i^{+1} \simeq 4 \times 10^{16}$ cm^{-3}, $T_e \simeq 5.0$ eV, and Joule and compressional heating rates of $5 \pm 1 \times 10^6$ and $4 \pm 2 \times 10^6$ W/cm^3, respectively, yields $v_f = 8 \pm 2 \times 10^6$ cm/s, which agrees well with the experimental value. As said previously, the validity of Eq. (6) is for the time interval $400 < t < 540$ ns. For these times, the variations in the values of the rhs terms of the equation are compensated by the particle density variations, which thus explains the nearly constant value of v_f observed.

Note that in this discussion photoionization was neglected since it was found to have a small effect on the ionization of O II. A calculation similar to that described above can be made for the propagation of the O III ionization, which is also supported by the Joule and compressional heatings. For this case, the radial velocities of O III and O IV
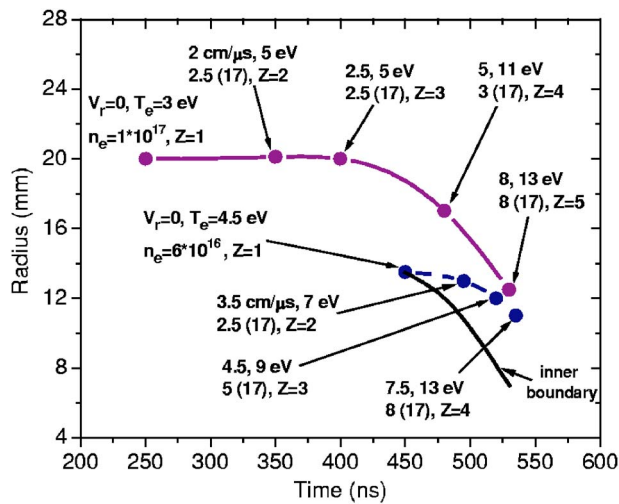
FIG. 7. Time history for the plasma parameters within two Lagrangian cells (see text). Given for each data point are the ion radial velocity, the electron temperature, the electron density, and the ion charge state. The times indicated for each data point are the times of the peak intensities of the respective emission lines, as obtained in end-on observations.

at $t \simeq 540$ ns, $\sim 2.5 \times 10^6$, and $\sim 5.0 \times 10^6$ cm/s, respectively, are used in the calculations, giving an ionization front velocity of $v_f = 5.0 \pm 1.5 \times 10^6$ cm/s, which agrees well with the experimental value of $\sim 6 \times 10^6$ cm/s.

Based on the complete r-t mapping of the measured parameters for the plasma under study, the ionization history in the plasma can be represented in Lagrangian coordinates, which may be useful in providing a basis for a future modeling of the plasma implosion. In such a representation, the plasma is divided into several fluid elements, and the particle ionization history within each element is tracked as the fluid element moves radially inward.

Consider a certain fluid element initially positioned at a radius r_0, for which its atoms are ionized into singly charged ions at the time t_0. In the laboratory frame of reference, the radial displacement history $r(t)$ of this element is obtained from

$$r(t) = r_0 + \int_{t_0}^{t} v_a[r(t'),t']dt', \qquad (7)$$

where $v[r(t'),t']$ is the measured radial velocity of the particles within the fluid element. This velocity, measured for each charge state,[5] vary in time as the particles ionize. The ionization times are thus required for the calculation of $r(t)$, and are obtained from Sec. IV. For each fluid element under consideration, the values of $n_e(t)$ and $T_e(t)$ are based on their measured radial distributions, and on the calculated $r(t)$.

Evidently, such a presentation of the plasma-parameter history can be made for any fluid element in the plasma. Here we only give two examples, as shown in Fig. 7. In the first case, we follow a fluid element for which $r_0 \simeq 20$ mm and $t_0 \sim 220$ ns, the latter being the time of initial observation of O II lines. The particles within this element ionize into O III, O IV, O V, and O VI at $t \sim 300$, ~ 370, ~ 490, and 530 ns, respectively, as indicated in the graph. In the second case, the fluid element is initially located at $r_0 = 13.5$ mm,

and is encountered by the ionization front at $t_0 \simeq 460$ ns. For this case, the ionization times are much shorter than those for the first element, and both elements are seen to merge at the outer plasma boundary at $t \simeq 540$ ns (the first element accelerates into the second one, see Fig. 7).

VI. SUMMARY

A method for determining the electron and ion densities in a Z-pinch plasma, based on the analysis of the particle ionization history within the imploding shell, is presented. The densities are determined by comparisons of the observed time-dependent radial charge-state distribution to that obtained from the results of a collisional-radiative modeling. In the calculations, the charge-state history is determined separately for each sublayer of the plasma shell, accounting for the ion radial-velocity distribution and the resulting mass transfer between the various sublayers. The electron density determined, together with the independently measured magnetic-field and electron-temperature distributions, are then used for studying the propagation of the ionization across the plasma shell. It is found that the initial ionization of neutrals ahead of the imploding shell results from photo-ionization by the continuum radiation from the dense plasma region, and that the continuous excitation and ionization of ions in the plasma is supported by the Joule heating and the compressional heating. The data allows for tracking the histories of the ionization, electron temperature, and radial velocity of any fluid element in the plasma, which is highly useful for the examination of magnetohydrodynamic modelings.

ACKNOWLEDGMENTS

[1] H. Sze, J. Banister, B. H. Failor *et al.*, *5th International Conference on Dense Z-Pinches*, Albuquerque, 23–28 June 2002, edited by J. Davis, C. Deeney, and N. R. Pereira, AIP Conf. Proc. No. 651 (AIP, Melville, NY, 2002), p. 101; J. W. Thornhill, J. P. Apruzese, J. Davis *et al.*, p. 105.

[2] D. D. Ryutov, M. S. Derzon, and M. K. Matzen, Rev. Mod. Phys. **72**, 167 (2000).

[3] M. A. Liberman, J. S. De Groot, A. Toor, and R. B. Spielman, *Physics of High-Density Z-Pinch Plasmas* (Springer, New York, 1999).

[4] D. Mosher, B. V. Weber, B. Moosman *et al.*, Laser Part. Beams **19**, 579 (2001).

[5] M. E. Foord, Y. Maron, G. Davara, L. Gregorian, and A. Fisher, Phys. Rev. Lett. **72**, 3827 (1994).

[6] H. R. Griem, *Spectral Line Broadening by Plasmas* (Academic, New York, 1974).

[7] H. R. Griem, *Principles of Plasma Spectroscopy* (Cambridge University Press, Cambridge, 1997).

[8] E. J. Iglesias and H. R. Griem, Phys. Rev. A **38**, 301 (1988).

[9] Yu. V. Ralchenko and Y. Maron, J. Quant. Spectrosc. Radiat. Transf. **71**, 609 (2001); R. Arad, K. Tsigutkin, Yu. V. Ralchenko, and Y. Maron, Phys. Plasmas **7**, 3797 (2000).

[10] L. Gregorian, E. Kroupp, G. Davara *et al.*, Phys. Rev. E **71**, 056402 (2005).

[11] G. Davara, L. Gregorian, E. Kroupp, and Y. Maron, Phys. Plasmas **5**,

1068 (1998).

[12] G. Davara, Ph.D. thesis, Feinberg Graduate School, Weizmnann Institute of Science (1995).

[13] F. C. Jahoda, E. M. Little, W. E. Quinn, G. A. Sawyer, and T. F. Stratton, Phys. Rev. **119**, 843 (1960).

[14] Ya. B. Zel'dovich and Yu. P. Raizer, *Physics of Shock Waves and High-Temperature Hydrodynamic Phenomena* (Academic, New York, 1967).

[15] J.-J. Yeh, *Atomic Calculation of Photoionization Cross-Sections and Asymmetry Parameters* (Gordon and Breach, Langhorne, PA, 1993).

[16] J. Davis, J. L. Giuliani, Jr., and M. Mulbrandon, Phys. Plasmas **2**, 1766 (1995).